Sodium-Ion Cathodes

Deutsche Ausgabe: DOI: 10.1002/ange.201411788
Internationale Ausgabe: DOI: 10.1002/anie.201411788

A Layered P2- and O3-Type Composite as a High-Energy Cathode for Rechargeable Sodium-Ion Batteries**

Shaohua Guo, Pan Liu, Haijun Yu, Yanbei Zhu, Mingwei Chen, Masayoshi Ishida, and Haoshen Zhou**

Abstract: *A layered composite with P2 and O3 integration is proposed toward a sodium-ion battery with high energy density and long cycle life. The integration of P2 and O3 structures in this layered oxide is clearly characterized by XRD refinement, SAED and HAADF and ABF-STEM at atomic resolution. The biphase synergy in this layered P2 + O3 composite is well established during the electrochemical reaction. This layered composite can deliver a high reversible capacity with the largest energy density of 640 mAh g^{-1}, and it also presents good capacity retention over 150 times of sodium extraction and insertion.*

Rechargeable sodium-ion batteries (SIBs) are regarded as a promising candidate for the next generation energy storage devices owing to the enormous supply of sodium. SIBs with similar chemical storage mechanism represent the most appealing alternative to their lithium-ion counterparts, and are expected to be low-cost and chemically sustainable. Many efforts have been made in search for electrode materials to improve sodium storage performance. Layered oxide compounds, polyanion compounds, and other electrode materials have been extensively investigated.[1] In particular, layered sodium oxide Na_xMO_2 (M is a transition metal) with reversible deintercalation and intercalation has aroused interest over recent years. Several Na_xMO_2 polytypes with O3, P2, and P3 structures can be obtained by chemical solid-state synthesis. According to the nomenclature proposed by Delmas et al., symbols of O or P denote the octahedral or prismatic environment for Na sites, and symbols of 2 or 3 indicates the minimum number of transition metal layers in the repeating cell unit.[2]

Among these layered sodium oxides, the P2 structure seems more attractive as a candidate for high-rate electrodes. Sodium ions can diffuse directly between two facing-sharing trigonal prismatic sites in the sodium layer (Supporting Information, Scheme S1), leading to better rate performance, which is consistent with the results of first-principle calculations.[3] When P2-type compounds serve as cathode, however, over-extraction of sodium at high voltage causes structural changes,[4] preventing full sodium reinsertion upon discharge and seriously limiting the reversible cycles. Based on the advanced in situ SXRD technique, Meng and co-workers reported that partial Li doping in a $Na_{0.8}Li_{0.12}Ni_{0.22}Mn_{0.66}O_2$ electrode could well inhibit the frequently observed P2–O2 phase transformation and retain a hexagonal P2-stacked structure even when the electrode is charged to 4.4 V.[5] Therefore, partial lithium substitution is an effective method to greatly enhance the structural stability of P2-type compounds.[6]

In comparison, the O3 phase (for example, Na/M = 1) is a sufficient sodium-ion reservoir, and can supply enough sodium, especially in full cells.[7] Many recent reports on binary or multinary O3-type compounds also show their high reversible capacity exceeding 150 mAh g^{-1},[8] which surpass other rivals as cathode of SIBs. In the same voltage range, the O3 phase shows much more reversible capacity than its P2 polytype in the Na_xMnO_2 system,[9] which is the same in Na_xVO_2 system.[10] However, intervention of intermediate sites in the sodium migration needs to overcome a high energy barrier for O3-type structure (Supporting Information, Scheme S1),[11] and inevitable complex phase transition and weak kinetics performance will directly influence the electrochemical properties.[8b,12] It is also found that the substituted lithium ions cannot suppress the O3–P′3 phase transition during electrochemical process in the high capacity O3-type $Na_{0.95}Li_{0.15}Ni_{0.15}Mn_{0.55}Co_{0.1}O_2$ cathode materials.[8c]

[*] S. Guo,[+] Dr. H. Yu, Prof. H. Zhou
Energy Technology Research Institute, National Institute of Advanced Industrial Science and Technology (AIST)
Umezono 1-1-1, Tsukuba, 305-8568 (Japan)
E-mail: haijun-yu@aist.go.jp
hs.zhou@aist.go.jp
S. Guo,[+] Prof. M. Ishida, Prof. H. Zhou
Graduate School of System and Information Engineering
University of Tsukuba, Tennoudai 1-1-1, Tsukuba, 305-8573 (Japan)
P. Liu,[+] Prof. M. Chen
WPI Advanced Institute for Materials Research
Tohoku University, Sendai 980-8577 (Japan)
Dr. Y. Zhu
National Metrology Institute of Japan
National Institute of Advanced Industrial Science and Technology (AIST) (Japan)
Prof. H. Zhou
National Laboratory of Solid State Microstructures &
Department of Energy Science and Engineering
Nanjing University, Nanjing 210093 (China)
[+] These authors contributed equally to this work.

[**] S.G. is grateful for financial support of the CSC (China Scholarship Council) scholarship. We thank Dr. Yang Sun for useful discussion and suggestions. This work was supported by the Innovative Basic Research toward Creation of High-performance Battery in Funding Program for World-leading Innovative R&D on Science and Technology. P.L. and M.C. are sponsored by the JST-CREST "Phase Interface Science for Highly Efficient Energy Utilization", JST (Japan).

Supporting information for this article is available on the WWW under http://dx.doi.org/10.1002/anie.201411788.

Recently, Johnson et al. successfully introduced mutiphase (P2, O′3, and P3) into O3-type $NaNi_{0.5}Mn_{0.5}O_2$ materials.[6b] Due to the multiphase's superiority, it well promote the smooth diffusion of sodium toward high power cathode.[6b] However, the O3–P3 phase transition in the O3-majority materials dominates during the cycling process, thus resulting in the weak cycling performance of 20 cycles and limited reversible capacity of 140 mAh g^{-1}. On basis of the above-mentioned ideas, we propose a novel design principle, namely integrating minor O3 into lithium-substituted P2-majority layered materials toward a large-capacity cathode material with an excellent rate and cycling performance.

Herein, O3 integration into lithium-substituted P2-majority in the P2 + O3 layered oxide composite ($Na_{0.66}Li_{0.18}Mn_{0.71}Ni_{0.21}Co_{0.08}O_{2+\delta}$, hereafter denoted as P2 + O3 NaLiMNC composite) is implemented through co-precipitation and subsequent solid-state reaction, and the biphase synergy in this layered P2 + O3 composite is well-established during the electrochemical reaction. The half cell of P2 + O3 NaLiMNC composite and sodium metal shows a large discharge capacity of 200 mAh g^{-1} at a 0.1 C rate, and the highest energy density of 640 Wh kg^{-1} to our knowledge. It can provide a capacity of 134 mAh g^{-1} at a discharge rate of 1 C (100 mA g^{-1}), which is related to enhanced rate capability. After 50 desodiation and sodiation processes at a 0.2 C rate, capacity retention of 84 % is achieved, showing good cycle stability. The superior sodium storage performance of layered P2 + O3 composite makes it promising candidate for large-scale energy storage devices.

The P2 compound (see the Supporting Information), which can be compared against, is characterized by powder X-ray diffraction (XRD) and scanning electron microscopy (SEM) in Figure S1. The XRD pattern in Figure S1a shows the purity of the P2 structure with space group $P6_3/mmc$, and the lattice parameters are refined to be $a = b = 2.8809(1)$ Å, $c = 11.0668(2)$ Å, and $V = 79.546(5)$ Å^3 with convergence factor s R-factors (11.80 %) and χ^2 (2.432) value using the GSAS + EXPGUI suite[13] (Detailed crystallographic data on refined P2-type are listed in the Supporting Information, Table S1). The P2 crystal structure is shown in Figure S1b, and SEM images in Figure S1c reveal that the particle size of the P2 NaLiMNC compound is in the range of 0.5–2 μm. The XRD pattern of P2 + O3 NaLiMNC composite is shown in Figure 1 a, and it indicates that most of the diffraction lines can be well indexed to a hexagonal lattice with space group $P6_3/mmc$, which is isostructural with the P2-type (JCPDS: 27-0751), and two other weak diffraction lines locating at 18.8° and 44.7°, which is assigned to O3-type structure (JCPDS: 09-0063) with space group $R\bar{3}m$. Rietveld refinement of the XRD pattern successfully gave reasonably low R-factors (4.45 %) and χ^2 (1.426) value based on P2 and O3 models.[13] P2 phase was fitted for lattice parameters of $a = b = 2.8721(1)$ Å, $c = 11.1663(2)$ Å and $V = 79.771(4)$ Å^3, and O3 phase was refined as lattice parameters of $a = b = 2.8548(9)$ Å, $c = 14.186(1)$ Å and $V = 100.13(5)$ Å^3. The calculated XRD patterns are in good agreement with the experimental data, which is also validated by the enlarged diffraction lines with angle area 30–50° in the inset of Figure 1 a. The detailed refinement results are shown in the Supporting Information, Table S2. Note that

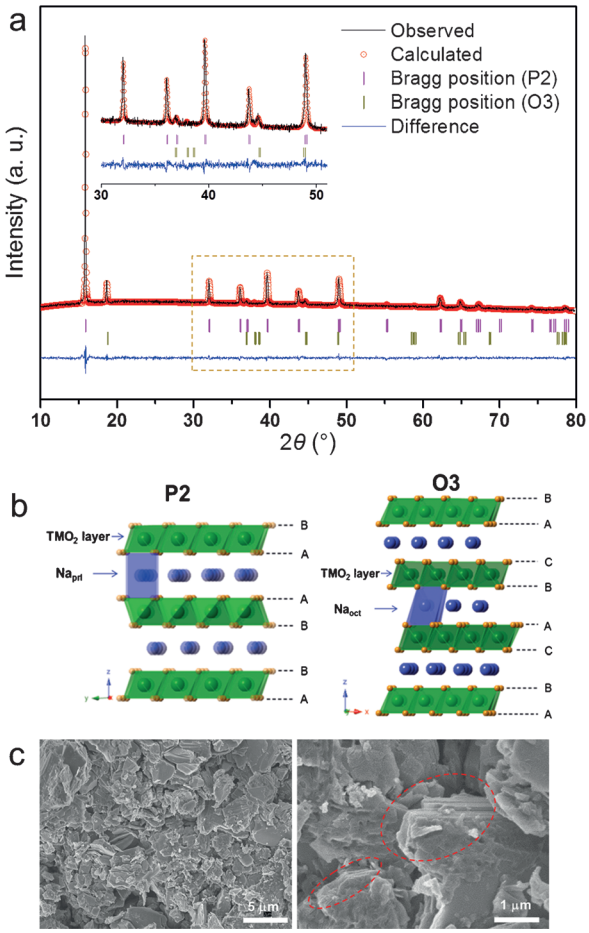

Figure 1. a) XRD patterns of P2 + O3 NaLiMNC composite and Rietveld refinement. The inset shows the enlarged diffraction area between 30° and 50°. b) The layered structures P2 (left) and O3 (right). c) SEM images of P2 + O3 NaLiMNC composite samples; red dotted lines show a sheet-like morphology of the P2 + O3 NaLiMNC composite.

there is a major difference between $c = 11.0668(2)$ Å in the P2 NaLiMNC compound and $c = 11.1663(2)$ Å of the P2 phase in the composite, indicating that the P2 major phase in composite has enlarged interlayer spacing and can supply open space for sodium-ion migration. This characteristic could be beneficial for activating more sodium ions and accelerating sodium-ion diffusion speed in P2 phase of this composite. The detailed electrochemical properties of the P2 + O3 NaLiMNC composite and the P2 NaLiMNC compound will be discussed in the following section.

Figure 1 b shows the crystal schematic of layered P2 (left) and O3 (right) structures. P2 and O3 are used to describe the ABBA and ABCABC stacking of oxygen layer respectively in Figure 1 b, and both of them are characterized by MO_6 edge-sharing octahedral units forming $(MO_2)_n$ sheets, can easily host sodium or lithium atoms, which occupy trigonal prismatic sites for P2 or octahedral sites for O3. Figure 1 c shows (SEM) images with different magnification of P2 + O3 NaLiMNC composite samples, and it is evident that P2 + O3 composite samples have the similar particle size with the P2 compound in left of Figure 1 c). Otherwise, some of P2 + O3 composite particles clearly display a sheet-like morphology in

right of Figure 1c, composed by lamellar stacking of the synthetic nanosheets (circled with red dotted lines). Energy dispersive spectroscopy (EDS) mapping is carried out in the white rectangle frame are exhibited in Figure 2. It can be clearly seen that the sodium, manganese, nickel, cobalt, and oxygen elements distributed in the particle uniformly. The lithium element is difficult to detect in P2 + O3 NaLiMNC composite owing to its weak X-ray scattering energy and low content.

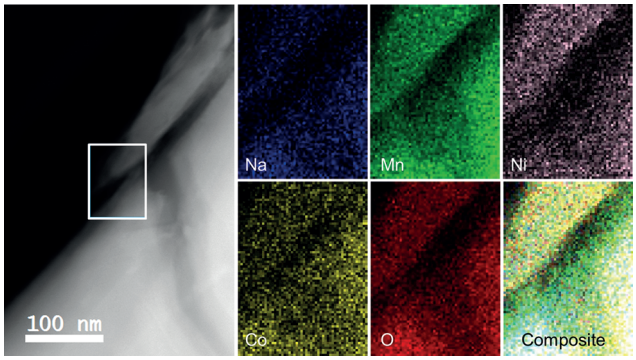

Figure 2. The EDS maps of P2 + O3 NaLiMNC composite samples, demonstrating an even distribution of sodium, manganese, nickel, cobalt, and oxygen elements in sample particles.

The separated O3 and P2 phases of the composite samples with an intergrowth interfaces are revealed for the scanning area electron diffraction (SAED) and scanning transmission electron microscopy (STEM) in Figure 3. The typical particle we chose for observations is shown in the Supporting Information, Figure S3. Figure 3a,b indicates the SAED patterns of the O3 phase and P2 phase, respectively. The bright spots of the O3 phase projected along the [010] direction in Figure 3a corresponds to a typical diffraction pattern for an O3-structure lattice. The bright spots projected along [100] direction in Figure 3b can be assigned to characteristic reflections originating from a P2-structure lattice. The simulated stacking sequences along *c*-axis crystallographic direction, indexed as typical reflections originating from layered O3-type and P2-type structure, perfectly match the experimental data (see also the Supporting Information, Figure S4).

The local structure of the P2 + O3 NaLiMNC composite was analyzed with atomic resolution by high-angle annular dark field (HAADF) and annular bright field (ABF)-STEM. Figure 3c,d shows representative HAADF-STEM and ABF-STEM images the nearby interface of P2- and O3-type phases respectively, indicating coherent orientation relationship by intergrowth of nanoscale domains. The bright-dot contrast in HAADF-STEM images (Figure 3c) and the dark-dot contrast in ABF-STEM images (Figure 3d) reveal the transition-metal (Mn, Ni and Co) atom column positions. The dark-dot contrast with the interlayer positions in ABF-STEM images (Figure 3d) corresponds to the alkali-metal Na/Li and oxygen atom column positions in these two layered structures. As shown in Figure 3e–h, the high resolution STEM images enlarged from blue and red frames of Figure 3c,d reveal the detailed atomic arrangements with regard to different O3 and P2 stacks respectively, and the atomic models of these two structures are inserted for ease of comparison. ABF-STEM observation of octahedral MO_2 (M = Mn/Ni/Co) are highly consistent with the structural model, as highlighted by green shade. The alkali metal atoms are clamped by layered MO_2. Specially, every two layers of MO_2 are mirror symmetric structurally and the head-to-head stacking model is observed for P2 phase, which is distinctly different with the layer distance of each O column in O3 phase. Furthermore, the corresponding fast Fourier transformation (FFT) images was shown in the inset of Figure 3g, indicative of a hexagonal lattice.

The coexistence between P2 and O3 phases is clearly characterized from macro to micro scale by the refined XRD,

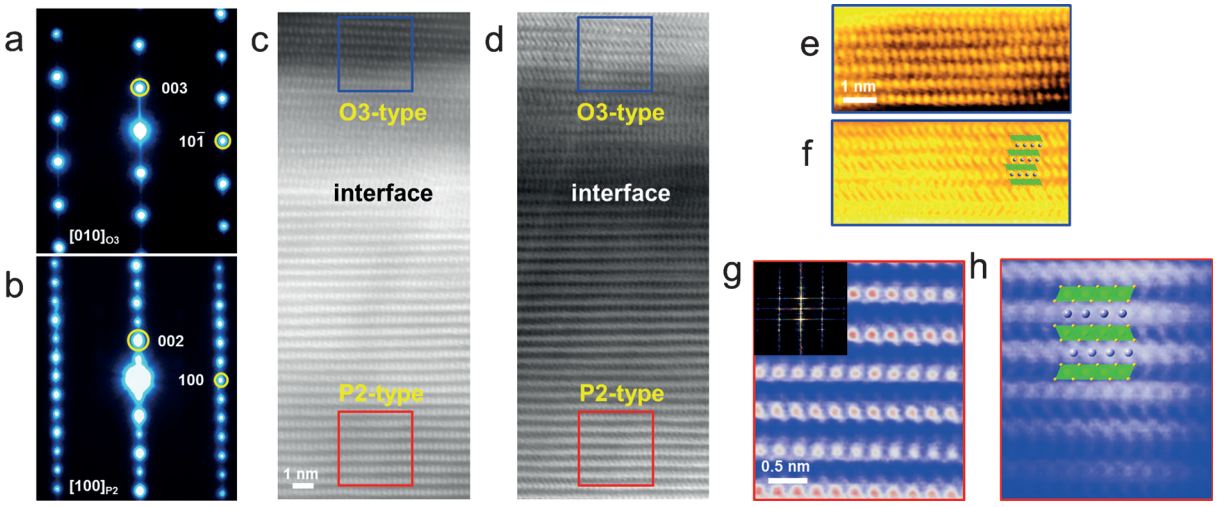

Figure 3. The SAED patterns of the P2 + O3 NaLiMNC composite: a) O3-type structure and b) P2-type structure; The STEM images: c) HADDF and d) ABF images of P2 + O3 NaLiMNC composite; the blue and red rectangle represent O3 structure and P2 structure areas. The enlarged images corresponding to the rectangle areas are shown in (e), (f), (g), and (h).

SEM, EDS maps, SAED, and STEM characterizations. The diphase integration is confirmed at atomic resolution, and this atomic-scale integration engineering would open up the modulation of the physical and chemical properties in layered P2 + O3 composite. The O3-structure integration and the enlarged P2 structure would have a profound impact on the electrochemical performance, just as $LiMO_2$ and Li_2MnO_3-like phases in the lithium-rich materials interplay.[14] The O3 phase can supply more sodium ions while the enlarged layered spacing of P2 phase is beneficial for easy diffusion of sodium ions upon charging process. Furthermore, Li-ion local chemical environment is unable to be captured by our current characterization. Johnson et al. and Meng et al. have investigated the lithium local environment of lithium-substituted P2 layered materials in detail using Li NMR spectroscropy.[3a,5] They found that most of lithium ions are present in the transition metal layer and partial lithium ions can be observed in the Na layer.

The electrochemical performances of the P2 + O3 NaLiMNC composite and P2 NaLiMNC compound in sodium half cells were evaluated with the voltage region of 1.5–4.5 V. Figure S2 (Supporting Information) shows the electrochemical properties of the P2 NaLiMNC compound, and only a reversible discharge capacity of 125 mAh g^{-1} was obtained, which performs equally with many other layered oxide solid solutions.[15] Not surprisingly, it showed good rate capability and stable cycling performance owing to the direct sodium diffusion and the structural stability of Li-substituted P2 structure. Figure 4a illustrates the typical charge–discharge profiles of a half-cell with the same voltage range of 1.5–4.5 V. It can be clearly seen that the initial discharge curves fully coincide with others, and a very large reversible discharge capacity of 200 mAh g^{-1} was obtained in the first cycle and subsequent cycles (Figure 4a; Supporting Information, Figure S5a) at a charge–discharge rate of 0.1 C. Meanwhile, the cyclic voltammogram (CV) curves are shown in the Supporting Information, Figure S5b. The CV curves show good consistency and reversibility in the subsequent cycles except for the initial activation process. Multiple redox peaks can be observed in the whole voltage range of 1.5–4.5 V. The low-voltage redox peak at about 2.0 V is probable associated with the redox process of manganese, the middle redox peaks in the region of about 2-3.9 V may be attributed to the redox couple of cobalt and the low valence state nickel, and the high-voltage redox peak above 4 V possibly corresponds to the redox reaction of the high valence state nickel.[16] On basis of its average voltage of 3.2 V, the energy density is calculated as 640 Wh kg^{-1}, a value that far surpasses that of other reported sodium battery cathodes and the commercial lithium battery cathodes, such as $LiFePO_4$ (about 530 Wh kg^{-1} versus Li) and $LiMn_2O_4$ (about 450 Wh kg^{-1}).[17] To the best of our knowledge, this material exhibits the highest energy density in all of the reported positive electrode materials for SIBs. It is clear that a high reversible capacity with the largest energy density is obtained through P2 and O3 interface engineering, which plays double roles in the enhanced electrochemical properties. O3 phase itself is a more sufficient sodium-ion reservoir, and enlargement of P2 layered spacing is beneficial for easy diffusion of sodium, would activate more sodium ions in the electrochemical reaction. Given that no additional sodium ions are supplied from the anode of the sodium full cells, the voltage is cut off in the region of 2–4.5 V (Supporting Information, Figure S6). It can be seen that this layered composite provides a reversible capacity of 143 mAh g^{-1} with

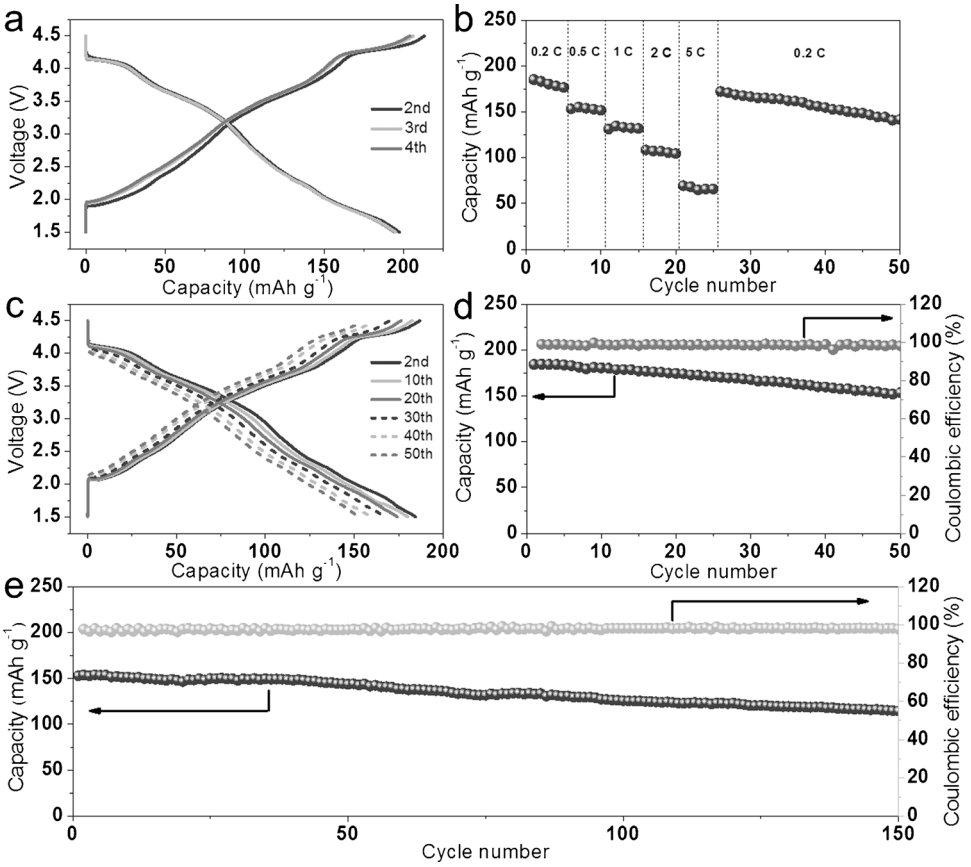

Figure 4. The electrochemical performance of the P2 + O3 NaLiMNC composite. a) The typical charge–discharge profiles between 1.5 and 4.5 V at a 0.1 C rate (1 C rate corresponding to 100 mA g^{-1}). b) The rate capability at different rates of 0.2 C, 0.5 C, 1 C, 2 C, and 5 C. c) The charge–discharge profiles in different 2nd, 10th, 20th, 30th, 40th, and 50th cycles with a rate of 0.2 C. d) The cycling performance with coulombic efficiency at a 0.2 C rate. e) The cycling performance with coulombic efficiency at a 0.5 C rate.

2–4.5 V at 0.2 C rate, and the high coincidence of the charge–discharge profiles except for the initial charge activation indicates good reversibility.

Rate capabilities of the P2 + O3 NaLiMNC composite/Na cells at rates of 0.2 C, 0.5 C, 1 C, 2 C, and 5 C are examined and shown in Figure 4b. The rate capability varies from 185 mAh g^{-1} at a 0.2C discharge rate to 134 mAh g^{-1} at a 1C discharge rate. Even with the a high rate of 5C (500 mA g^{-1}), the sodium half-cell consisting of the P2 + O3 composite cathode and sodium metal still supply an acceptable reversible capacity of 69 mAh g^{-1}. Furthermore, the almost complete recovery of discharge capacity when returning to the 0.2 C rate, gives a further evidence for the structural stability of electrode materials. It is generally considered that the fast sodium migration can be achieved between trigonal prismatic sites in P2-majority composite during the entire range of the charge–discharge process.

The cycling performance and the corresponding coulombic efficiency are firstly tested with a rate of 0.2 C and shown in Figure 4d, and the corresponding charge–discharge profile at different cycles are displayed in Figure 4c. The half-cell offers 84% capacity retention for 50 desodiation and sodiation processes, and the large capacity, the enhanced cycle life, and well-defined voltage plateau match well those expected by a structurally optimized, lithium-substituted P2 majority with high structural stability. Note that other layered materials can even deliver a large capacity approaching 200 mAh g^{-1}, but limited cycles of 20 or 30 times desodiation and sodiation with about 70% capacity retention are obtained in the current development stage of sodium battery cathodes.[1n,4a] To further study the long-term cycling performance, the sodium half-cell is evaluated for 150 cycles at a 0.5 C rate (Figure 4e). In the deep charging and discharging status, a good capacity retention of 75% is measured even after 150 cycles of sodium ion extraction and insertion. High coulombic efficiency is regarded as an important feature for the potential of practical application. For this material, the coulombic efficency in the whole cycling process is about close to 98.5% except for the initial cycle and a few special cycles, which is suitable to serve as a sodium cathode in practical applications.

In summary, a novel layered composite material with P2 + O3 structural integration is synthesized through co-precipitation and subsequent solid-state reaction. The novel P2 + O3 NaLiMNC composite material as cathode of SIBs shows excellent electrochemical performance, and in particular presents a large discharge capacity (200 mAh g^{-1}), good rate capability (a large discharge capacity of 134 mAh g^{-1} at a high rate of 1 C), and good cycling stability (84% capacity retention after 50 cycles at 0.2 C rate and 75% capacity retention after 150 cycles at a 0.5 C rate), which is superior to other layered materials. With the average voltage of 3.2 V, the energy density of this material is calculated as approximately 640 Wh kg^{-1}, which is the largest value of all the reported positive electrode materials for SIBs, and is comparable to the state-of-the-art lithium-ion batteries. The superior sodium storage performance of layered P2 + O3 composite makes it promising candidate for large-scale energy storage devices. This strategy of P2 and O3 integration expand a deeper understanding the structure–electrochemical property relationships, and also provide new avenues for designing cathode materials with superior comprehensive performance. Further work on the interplay mechanism and optimal distributions between O3 and P2 phases in the composite structure is under investigation.

Keywords: layered structures · composite materials · Na_xMO_2 polytypes · sodium-ion cathodes

How to cite: *Angew. Chem. Int. Ed.* **2015**, *54*, 5894–5899
Angew. Chem. **2015**, *127*, 5992–5997

[1] a) S. W. Kim, D. H. Seo, X. Ma, G. Ceder, K. Kang, *Adv. Energy Mater.* **2012**, *2*, 710–721; b) P. Barpanda, G. Oyama, C. D. Ling, A. Yamada, *Chem. Mater.* **2014**, *26*, 1297–1299; c) S. Wang, L. Wang, Z. Zhu, Z. Hu, Q. Zhao, J. Chen, *Angew. Chem. Int. Ed.* **2014**, *53*, 5892–5896; *Angew. Chem.* **2014**, *126*, 6002–6006; d) J. Qian, X. Wu, Y. Cao, X. Ai, H. Yang, *Angew. Chem. Int. Ed.* **2013**, *52*, 4633–4636; *Angew. Chem.* **2013**, *125*, 4731–4734; e) D. Su, G. Wang, *ACS Nano* **2013**, *7*, 11218–11226; f) W.-J. Li, S.-L. Chou, J.-Z. Wang, H.-K. Liu, S.-X. Dou, *Nano Lett.* **2013**, *13*, 5480–5484; g) Y. Yan, Y. X. Yin, Y. G. Guo, L. J. Wan, *Adv. Energy Mater.* **2014**, *4*, 1301584; h) Z. Jian, W. Han, X. Lu, H. Yang, Y. S. Hu, J. Zhou, Z. Zhou, J. Li, W. Chen, D. Chen, *Adv. Energy Mater.* **2013**, *3*, 156–160; i) Y.-U. Park, D.-H. Seo, H.-S. Kwon, B. Kim, J. Kim, H. Kim, I. Kim, H.-I. Yoo, K. Kang, *J. Am. Chem. Soc.* **2013**, *135*, 13870–13878; j) S. Y. Lim, H. Kim, J. Chung, J. H. Lee, B. G. Kim, J.-J. Choi, K. Y. Chung, W. Cho, S.-J. Kim, W. A. Goddard, *Proc. Natl. Acad. Sci. USA* **2014**, *111*, 599–604; k) Y. Yue, A. J. Binder, B. Guo, Z. Zhang, Z. A. Qiao, C. Tian, S. Dai, *Angew. Chem. Int. Ed.* **2014**, *53*, 3134–3137; *Angew. Chem.* **2014**, *126*, 3198–3201; l) Y. You, X.-L. Wu, Y.-X. Yin, Y.-G. Guo, *Energy Environ. Sci.* **2014**, *7*, 1643–1647; m) S. Guo, H. Yu, P. Liu, Y. Ren, T. Zhang, M. Chen, M. Ishida, H. Zhou, *Energy Environ. Sci.* **2015**, DOI: 10.1039/c4ee03361b; n) S. Guo, H. Yu, Z. Jian, P. Liu, Y. Zhu, X. Guo, M. Chen, M. Ishida, H. Zhou, *ChemSusChem* **2014**, *7*, 2115–2119; o) H. Yu, Y. Ren, D. Xiao, S. Guo, Y. Zhu, Y. Qian, L. Gu, H. Zhou, *Angew. Chem. Int. Ed.* **2014**, *53*, 8963–8969; *Angew. Chem.* **2014**, *126*, 9109–9115; p) T. Zhou, W. K. Pang, C. Zhang, J. Yang, Z. Chen, H. K. Liu, Z. Guo, *ACS Nano* **2014**, *8*, 8323–8333; q) H. Pan, Y.-S. Hu, L. Chen, *Energy Environ. Sci.* **2013**, *6*, 2338–2360; r) Y. Sun, L. Zhao, H. Pan, X. Lu, L. Gu, Y.-S. Hu, H. Li, M. Armand, Y. Ikuhara, L. Chen, *Nat. Commun.* **2013**, *4*, 1870; s) S. Xu, X. Wu, Y, Li, Y. Hu, L. Chen, *Chin. Phys. B* **2014**, *23*, 118202; t) L. Mu, Y. Hu, L. Chen, *Chin. Phys. B* **2015**, *24*, 038202.

[2] C. Delmas, C. Fouassier, P. Hagenmuller, *Physica B + C* **1980**, *99*, 81–85.

[3] a) N. K. Karan, M. D. Slater, F. Dogan, D. Kim, C. S. Johnson, M. Balasubramanian, *J. Electrochem. Soc.* **2014**, *161*, A1107–A1115; b) S. P. Ong, V. L. Chevrier, G. Hautier, A. Jain, C. Moore, S. Kim, X. Ma, G. Ceder, *Energy Environ. Sci.* **2011**, *4*, 3680–3688; c) D. H. Lee, J. Xu, Y. S. Meng, *Phys. Chem. Chem. Phys.* **2013**, *15*, 3304–3312.

[4] a) N. Yabuuchi, M. Kajiyama, J. Iwatate, H. Nishikawa, S. Hitomi, R. Okuyama, R. Usui, Y. Yamada, S. Komaba, *Nat. Mater.* **2012**, *11*, 512–517; b) I. Hasa, D. Buchholz, S. Passerini, B. Scrosati, J. Hassoun, *Adv. Energy Mater.* **2014**, *4*, 1400083.

[5] J. Xu, D. H. Lee, R. J. Clément, X. Yu, M. Leskes, A. J. Pell, G. Pintacuda, X.-Q. Yang, C. P. Grey, Y. S. Meng, *Chem. Mater.* **2014**, *26*, 1260–1269.

[6] a) D. Kim, S. H. Kang, M. Slater, S. Rood, J. T. Vaughey, N. Karan, M. Balasubramanian, C. S. Johnson, *Adv. Energy Mater.* **2011**, *1*, 333–336; b) E. Lee, J. Lu, Y. Ren, X. Luo, X. Zhang, J. Wen, D. Miller, A. DeWahl, S. Hackney, B. Key, *Adv. Energy Mater.* **2014**, *4*, 1400458; c) N. Yabuuchi, R. Hara, M. Kajiyama,

K. Kubota, T. Ishigaki, A. Hoshikawa, S. Komaba, *Adv. Energy Mater.* **2014**, *4*, 1301453.
[7] C. Fouassier, C. Delmas, P. Hagenmuller, *Mater. Res. Bull.* **1975**, *10*, 443 – 449.
[8] a) H. Yoshida, N. Yabuuchi, S. Komaba, *Electrochem. Commun.* **2013**, *34*, 60 – 63; b) S. Komaba, N. Yabuuchi, T. Nakayama, A. Ogata, T. Ishikawa, I. Nakai, *Inorg. Chem.* **2012**, *51*, 6211 – 6220; c) S.-M. Oh, S.-T. Myung, J.-Y. Hwang, B. Scrosati, K. Amine, Y.-K. Sun, *Chem. Mater.* **2014**, *26*, 6165; d) X. Sun, Y. Jin, C.-Y. Zhang, J.-W. Wen, Y. Shao, Y. Zang, C.-H. Chen, *J. Mater. Chem. A* **2014**, *2*, 17268 – 17271; e) P. Vassilaras, A. J. Toumar, G. Ceder, *Electrochem. Commun.* **2014**, *38*, 79 – 81; f) R. Kataoka, T. Mukai, A. Yoshizawa, T. Sakai, *J. Electrochem. Soc.* **2013**, *160*, A933 – A939.
[9] a) A. Caballero, L. Hernan, J. Morales, L. Sanchez, J. S. Pena, M. Aranda, *J. Mater. Chem.* **2002**, *12*, 1142 – 1147; b) X. Ma, H. Chen, G. Ceder, *J. Electrochem. Soc.* **2011**, *158*, A1307 – A1312.
[10] D. Hamani, M. Ati, J.-M. Tarascon, P. Rozier, *Electrochem. Commun.* **2011**, *13*, 938 – 941.
[11] S. Pingáng, *Phys. Chem. Chem. Phys.* **2012**, *14*, 15571 – 15578.
[12] a) S. Komaba, T. Nakayama, A. Ogata, T. Shimizu, C. Takei, S. Takada, A. Hokura, I. Nakai, *ECS Trans.* **2009**, *16*, 43 – 55; b) M. Sathiya, K. Hemalatha, K. Ramesha, J.-M. Tarascon, A. Prakash, *Chem. Mater.* **2012**, *24*, 1846 – 1853; c) S.-M. Oh, S.-T. Myung, C. S. Yoon, J. Lu, J. Hassoun, B. Scrosati, K. Amine, Y.-K. Sun, *Nano Lett.* **2014**, *14*, 1620 – 1626; d) P. Vassilaras, X. Ma, X. Li, G. Ceder, *J. Electrochem. Soc.* **2013**, *160*, A207 – A211; e) J. Braconnier, C. Delmas, P. Hagenmuller, *Mater. Res. Bull.* **1982**, *17*, 993 – 1000.
[13] a) A. C. Larson, R. B. Von Dreele, General Structure Analysis System, LANSCE, MS-H805, Los Alamos, New Mexico **1994**; b) B. H. Toby, *J. Appl. Crystallogr.* **2001**, *34*, 210 – 213.
[14] H. Yu, R. Ishikawa, Y. G. So, N. Shibata, T. Kudo, H. Zhou, Y. Ikuhara, *Angew. Chem. Int. Ed.* **2013**, *52*, 5969 – 5973; *Angew. Chem.* **2013**, *125*, 6085 – 6089.
[15] a) H. Yu, S. Guo, M. Ishida, Z. Yanbei, H. Zhou, *Chem. Commun.* **2014**, *50*, 457 – 459; b) I. Saadoune, A. Maazaz, M. Menetrier, C. Delmas, *J. Solid State Chem.* **1996**, *122*, 111 – 117; c) Z. H. Lu, J. R. Dahn, *J. Electrochem. Soc.* **2001**, *148*, A1225 – A1229; d) M. B. Sassin, C. P. Hoag, B. T. Willis, N. W. Kucko, D. R. Rolison, J. W. Long, *Nanoscale* **2013**, *5*, 1649 – 1657; e) S. Guo, H. Yu, W. Tian, X. Liu, N. Hanada, M. Ishida, H. Zhou, *Chem. Commun.* **2014**, *50*, 7998 – 8001.
[16] a) J. Thorne, R. Dunlap, M. Obrovac, *J. Electrochem. Soc.* **2013**, *160*, A361 – A367; b) D. Yuan, X. Hu, J. Qian, F. Pei, F. Wu, R. Mao, X. Ai, H. Yang, Y. Cao, *Electrochim. Acta* **2014**, *116*, 300 – 305; c) J.-H. Cheng, C.-J. Pan, J.-F. Lee, J.-M. Chen, M. Guignard, C. Delmas, D. Carlier, B.-J. Hwang, *Chem. Mater.* **2014**, *26*, 1219 – 1225; d) N. Yabuuchi, R. Hara, M. Kajiyama, K. Kubota, T. Ishigaki, A. Hoshikawa, S. Komaba, *Adv. Energy Mater.* **2014**, *4*, 1301453.
[17] a) J. Liu, M. N. Banis, Q. Sun, A. Lushington, R. Li, T. K. Sham, X. Sun, *Adv. Mater.* **2014**, *26*, 6472 – 6477; b) Y. Wang, Y. Wang, E. Hosono, K. Wang, H. Zhou, *Angew. Chem. Int. Ed.* **2008**, *47*, 7461 – 7465; *Angew. Chem.* **2008**, *120*, 7571 – 7575; c) E. Hosono, T. Kudo, I. Honma, H. Matsuda, H. Zhou, *Nano Lett.* **2009**, *9*, 1045 – 1051.

Received: December 11, 2014
Revised: February 12, 2015
Published online: April 1, 2015

